Thin-Walled Structures 66 (2013) 62–75

Contents lists available at SciVerse ScienceDirect

Thin-Walled Structures

journal homepage: www.elsevier.com/locate/tws

Experimental behaviour of recycled aggregate concrete filled stainless steel tube stub columns and beams

You-Fu Yang *, Guo-Liang Ma

State Key Laboratory of Coastal and Offshore Engineering, Dalian University of Technology, Dalian 116024, China

ARTICLE INFO

Article history:
Received 8 June 2012
Received in revised form
8 October 2012
Accepted 22 January 2013
Available online 28 March 2013

Keywords:
Recycled aggregate concrete filled stainless steel tube (RACFSST)
Stub columns
Beams
Bearing capacity
Stiffness
Design code

ABSTRACT

The behaviour of recycled aggregate concrete (RAC) filled stainless steel tube (RACFSST) stub columns and beams under short-term loadings was experimentally studied, and a total of 28 specimens, including 14 stub columns and 14 beams, were tested. The experimental investigations were carried out on circular and square specimens with recycled aggregate replacement ratio of 0, 25%, 50% and 75%, and both recycled coarse aggregate (RCA) and recycled fine aggregate (RFA) were adopted in the tests. The main objectives of these tests were threefold: first, to describe a series of tests on new composite stub columns and beams; second, to investigate the effect of cross-section type and recycled aggregate replacement ratio on the compressive and flexural behaviour of RACFSST specimens; and finally, to evaluate the accuracy of the calculated bearing capacity, bending moment capacity and section flexural stiffness of the RACFSST specimens by using the design formulae in six codes related to the design of concrete filled carbon steel tube. The experimental results showed that the RACFSST stub columns and beams under short-term loadings had the stable load versus deformation responses and the good deformation-resistant ability, and the performance of core RAC was generally enhanced due to the confinement of the outer stainless steel tube.

1. Introduction

Stainless steel tube has a beautiful appearance, good durability, low-cost maintenance and good fire resistance, and it has good prospects of application in the buildings and bridges under marine environment and the important buildings requiring high aesthetics and durability. Although the stainless steel tube has superior performance, it cannot be applied largely in the structures due to the drawback of expensive cost. As a result, filling concrete into stainless steel tube, which is so-called concrete filled stainless steel tube (CFSST), is considered to be a good choice for structural application of stainless steel. CFSST can cause a significant reduction in the amount of stainless steel, so as to achieve the purpose of reducing the project cost. At the same time, the stability of the thin-walled stainless steel tube can be improved due to the existence of core concrete [1].

In recent years, CFSST has been used in several projects [1], and the performance of circular and square CFSST columns with or without inner stiffeners has been experimentally and theoretically studied, as summarised and presented in [2]. Furthermore, Feng and Young [3–5] experimentally and theoretically investigated the behaviour of CFSST T- and X-joints, and the simplified design formulae for such composite joints were suggested. Dai and Lam [6] and Lam et al. [7] presented the experimental and finite element modelling results of concrete filled stainless steel elliptical hollow sections, and the simplified equations for the bearing capacity prediction of such composite sections were also proposed. Tao et al. [8] developed a three-dimensional nonlinear finite element model for the analysis of square CFSST stub columns subjected to axial compression.

Production of recycled aggregates by recycling of the waste concrete can promote the reuse of waste concretes and further protect the natural aggregate resources. However, the quality of recycled aggregates produced from waste concrete from different sources has a greater randomness and variability. Recycling of waste concrete to produce structural grade concrete for major construction is technically feasible [9] provided that: (1) the clean, crushed and well-graded recycled aggregates are produced; (2) the grading of recycled aggregates can be brought within certain grading limits; (3) the recycled aggregates can pass the requirements for abrasion loss percentage or crushing value; and (4) the recycled aggregates can comply with maximum allowable limits on the content of contaminants. Moreover, the density and water absorption of recycled aggregates should be carefully determined before designing a mix of recycled aggregate concrete (RAC). In general, RAC has a lower performance compared with the corresponding normal concrete (NC) under the same mix proportion [9], and the application of RAC in building structures is

* Corresponding author. Tel.: +86 411 84708510; fax: +86 411 84674141.
E-mail address: youfuyang@163.com (Y.-F. Yang).

0263-8231/$ - see front matter © 2013 Elsevier Ltd. All rights reserved.
http://dx.doi.org/10.1016/j.tws.2013.01.017

Nomenclature

BRF	bearing capacity reduction factor
CFSST	concrete filled stainless steel tube
D	outside diameter or width of circular or square stainless steel tube
E_c	elastic modulus of concrete
ERF	elastic modulus reduction factor
E_{sc}	elastic modulus of composite stub column
f_{cu}	cube compressive strength of concrete
K_{ic}	calculated initial section flexural stiffness
K_{ie}	experimental initial section flexural stiffness
K_{sc}	calculated serviceability-level section flexural stiffness
K_{se}	experimental serviceability-level section flexural stiffness
M	bending moment
MRF	bending moment reduction factor
M_{uc}	calculated bending moment capacity
M_{ue}	experimental bending moment capacity
N	axial load
NC	normal concrete
NCA	natural coarse aggregate
N_{uc}	calculated bearing capacity of stub column
N_{ue}	experimental bearing capacity of stub column
r	recycled aggregate replacement ratio
RAC	recycled aggregate concrete
RACFSST	recycled aggregate concrete filled stainless steel tube
RCA	recycled coarse aggregate
RFA	recycled fine aggregate
SRF_i	initial section flexural stiffness reduction factor
SRF_s	serviceability-level section flexural stiffness reduction factor
t	wall thickness of stainless steel tube
u_m	mid-span deflection of the beam
ε	strain
ϕ	curvature
σ	stress

still rare. Filling RAC into steel tube is believed to be a solution for the structural use of RAC. The studies on RAC filled carbon steel tube members subjected to short-term static loadings [10,11], long-term sustained loads [12,13] and cyclic loadings [14,15] had recently been carried out. The results showed that RAC filled carbon steel tube members generally had the similar structural properties as the traditional concrete filled carbon steel tube members. RAC filled stainless steel tube (RACFSST) is a new kind of composite structure, and the durability of the structures with RACFSST can be greatly improved. Similar to RAC filled carbon steel tube, RACFSST also makes the RAC to be in a state of protection with the outer stainless steel tube, and core RAC is less likely to be affected by the harmful environmental factors (e.g. water, temperature and wind). Furthermore, RACFSST can broaden the application area of stainless steel. To date, there is no information for the structural behaviour of RACFSST members.

The aim of the present study is to experimentally investigate the structural behaviour of RACFSST stub columns and beams under short-term loadings, and the results of 28 specimens, including 14 stub columns and 14 beams, are presented and analysed. Both recycled coarse aggregate (RCA) and recycled fine aggregate (RFA) were considered in the tests, and the recycled aggregate replacement ratio (r) varied from 0 to 75%. The experimental results showed that the RACFSST stub columns and beams still had the stable load versus deformation responses and the good deformation-resistant ability. The accuracy of the calculated bearing capacity, bending moment capacity and flexural stiffness of RACFSST specimens by using the design formulae in ACI 318-05 [16], AIJ [17], ANSI/AISC 360-05 [18], BS 5400-5 [19], DB21/T1746-2009 [20] and EC4 [21] was evaluated based on the comparison with the experimental results.

2. Experimental investigations

2.1. Test specimens

Twenty-eight composite specimens, including 14 stub columns and 14 beams, were experimentally investigated in this study. Fig. 1 shows the cross section of the specimens, where D is the outside diameter or width of circular or square stainless steel tube, respectively, and t is the wall thickness of stainless steel tube. All specimens have the same diameter (width) to wall thickness ratio. The main parameters varied in the tests include: (1) cross-section of stainless steel tube: circular and square, and (2) r: 0 (CFSST), 25%, 50% and 75%. Both RCA and RFA are considered in the tests, and r is defined as the ratio of RCA or RFA mass to the mass of all coarse or fine aggregate, respectively.

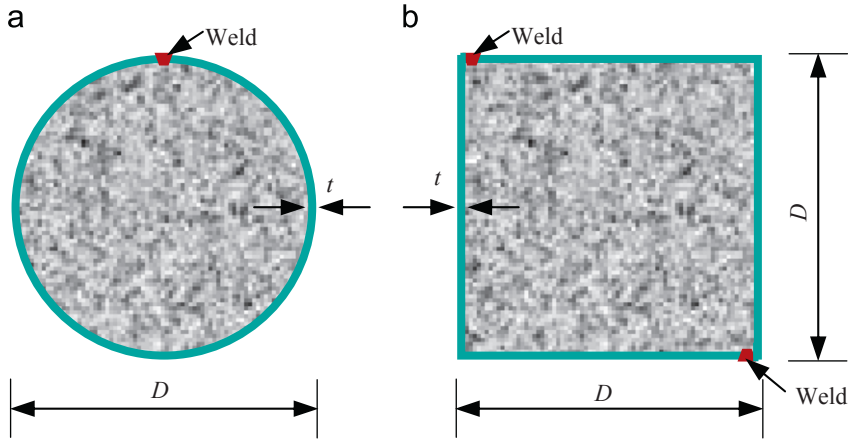

Fig. 1. Cross section of the specimens. (a) Circular section. (b) Square section.

Table 1
Information of the stub specimens.

Section type	No.	Specimen label	$D \times t$ (mm)	r (%)	E_{sc} (N/mm^2)	N_{ue} (kN)	ERF (%)	BRF (%)
Circular	1	C–S–N	○ – 120 × 1.77	0	40,828	823.2	0	0
	2	C–S–C1	○ – 120 × 1.77	25	38,351	813.8	−6.1	−1.1
	3	C–S–C2	○ – 120 × 1.77	50	36,888	802.2	−9.7	−2.6
	4	C–S–C3	○ – 120 × 1.77	75	34,867	774.3	−14.6	−5.9
	5	C–S–F1	○ – 120 × 1.77	25	37,019	806.7	−9.3	−2.0
	6	C–S–F2	○ – 120 × 1.77	50	35,373	768.4	−13.4	−6.7
	7	C–S–F3	○ – 120 × 1.77	75	33,861	777.2	−17.1	−5.6
Square	1	S–S–N	□ – 120 × 1.77	0	34,709	923.4	0	0
	2	S–S–C1	□ – 120 × 1.77	25	32,093	871.5	−7.5	−5.6
	3	S–S–C2	□ – 120 × 1.77	50	30,077	848.5	−13.3	−8.1
	4	S–S–C3	□ – 120 × 1.77	75	28,446	830.0	−18.0	−10.1
	5	S–S–F1	□ – 120 × 1.77	25	31,404	857.1	−9.5	−7.2
	6	S–S–F2	□ – 120 × 1.77	50	29,100	826.9	−16.2	−10.5
	7	S–S–F3	□ – 120 × 1.77	75	26,351	831.1	−24.1	−10.0

Table 2
Information of the beam specimens.

Section type	No.	Specimen label	$D \times t$ (mm)	r (%)	K_{ie} (kN.m^2)	K_{se} (kN.m^2)	M_{ue} (kN.m)	SRF$_i$ (%)	SRF$_s$ (%)	MRF (%)
Circular	1	C–B–N	○ – 120 × 1.77	0	320.5	196.2	11.72	0	0	0
	2	C–B–C1	○ – 120 × 1.77	25	311.8	189.3	11.57	−2.7	−3.5	−1.3
	3	C–B–C2	○ – 120 × 1.77	50	292.3	176.2	11.56	−8.8	−10.2	−1.4
	4	C–B–C3	○ – 120 × 1.77	75	277.1	179.5	11.54	−13.5	−8.5	−1.5
	5	C–B–F1	○ – 120 × 1.77	25	302.8	181.4	11.51	−5.5	−7.5	−1.8
	6	C–B–F2	○ – 120 × 1.77	50	285.3	172.1	10.63	−11.0	−12.3	−9.3
	7	C–B–F3	○ – 120 × 1.77	75	276.2	168.8	10.60	−13.8	−14.0	−9.6
Square	1	S–B–N	□ – 120 × 1.77	0	424.0	319.3	15.23	0	0	0
	2	S–B–C1	□ – 120 × 1.77	25	397.2	293.3	14.65	−6.3	−8.1	−3.8
	3	S–B–C2	□ – 120 × 1.77	50	366.5	290.8	14.31	−13.6	−8.9	−6.0
	4	S–B–C3	□ – 120 × 1.77	75	374.9	287.2	14.36	−11.6	−10.1	−5.7
	5	S–B–F1	□ – 120 × 1.77	25	387.6	285.8	14.55	−8.6	−10.5	−4.5
	6	S–B–F2	□ – 120 × 1.77	50	353.7	277.9	14.25	−16.6	−13.0	−6.4
	7	S–B–F3	□ – 120 × 1.77	75	340.4	269.4	13.63	−19.7	−15.6	−10.5

Each RAC has only one type of recycled aggregate. For all specimens, the stainless steel plate was selected to manufacture the tubes by machining and welding. The information of the stub and beam specimens investigated in the tests was presented in Tables 1 and 2, respectively. In Tables 1 and 2, the first capital letters 'C' and 'S' in specimen label denote circular and square stainless steel tube, respectively, and the second capital letters 'S' and 'B' indicate the stub and beam specimens, respectively. The last part of the label represents the type of core concrete. Each tube was welded to two circular (for circular sections) or square (for square sections) carbon steel base plate 12 mm thick.

The thin-walled plate of austenitic stainless steel type AISI 304 was used to produce the tube. The properties of stainless steel were obtained by testing three tensile coupons randomly taken from the plate. The measured stress (σ) versus strain (ε) relations of stainless steel are illustrated in Fig. 2. It can be seen that three curves have the similar trends and the main difference between them is the elongation at rupture. From the tests, the average yield strength (0.2% proof stress), tensile strength, modulus of elasticity and Poisson's ratio of stainless steel were found to be 286.7 MPa, 789.6 MPa, 1.85×10^5 N/mm^2 and 0.276, respectively. The average strain at rupture (elongation), which reflects the ductility of stainless steel, is 72.7% with standard deviation of 4.4%.

RCA and RFA were obtained by crushing the waste concrete in the laboratory using a small jaw crusher, and the cube compressive strength of the waste concrete was about 60 MPa. The maximum size of RCA and natural coarse aggregate (NCA) was 20 mm and 25 mm, and the water absorption of RCA and NCA

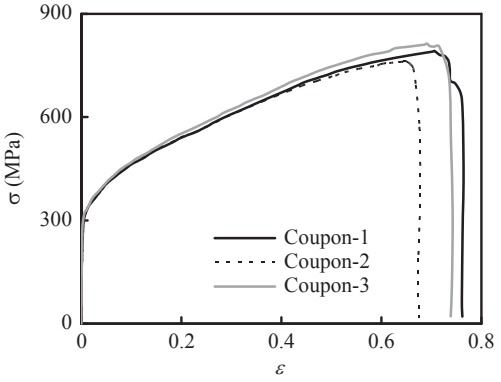

Fig. 2. Stress (σ) versus strain (ε) relations of stainless steel.

was 8.49% and 0.78%, respectively. The crushing value of RCA and NCA was 11.5% and 29.4%, respectively. The fineness modulus of RFA and natural sand was 3.0 and 2.7, and the water absorption of RFA and natural sand was 8.3% and 1.6%, respectively. It was found that, similar to the results presented in [9], the recycled aggregates were somewhat coarser and more angular than the natural aggregates, and to bring the recycled aggregates within the grading limits a certain amount of natural aggregates should be blended in.

Seven types of concrete, including one type of NC with natural aggregates, three types of RAC with 25%, 50% and 75% RCA, and three types of RAC with 25%, 50% and 75% RFA, were produced in

Table 3
The mix proportions and properties of new concrete.

Type	Label	r (%)	Mix proportions (kg/m^3)							Properties			
			Cement	Sand	RFA	NCA	RCA	Water	WRA	Slump (mm)	$f_{cu,28}$ (MPa)	$f_{cu,test}$ (MPa)	E_c (N/mm^2)
NC	N	0	473	636	–	1072	–	213.3	2.84	170	55.7	63.4	37,600
RAC	C1	25	473	636	–	804	268	213.3	2.84	110	53.0	59.7	35,300
	C2	50	473	636	–	536	536	213.3	2.84	80	51.1	57.3	33,600
	C3	75	473	636	–	268	804	313.3	2.84	30	50.4	56.9	30,500
	F1	25	473	477	159	1072	–	213.3	2.84	165	52.0	58.6	32,700
	F2	50	473	318	318	1072	–	213.3	2.84	145	49.2	56.2	30,300
	F3	75	473	159	477	1072	–	213.3	2.84	120	48.5	55.3	27,800

the tests. The mix proportions of all concrete were fixed, and the reference NC was designed for mean cube compressive strength at 28-day of approximately 50 MPa. Moreover, the water reducing agent (WRA) was added to ensure the workability of the concrete incorporating the recycled aggregates. To obtain the cube compressive strength (f_{cu}) and elastic modulus (E_c) of concrete, several 150 mm cubes and 150 mm × 300 mm prisms were cast and cured in conditions similar to the composite specimens. The mix proportions and properties of new concrete are presented in Table 3, where $f_{cu,28}$ and $f_{cu,test}$ are the mean cube compressive strength at 28 days and when the loading tests were conducted, respectively. It is shown that, the slump of new concrete decreases with increase of r, and RAC containing RCA resulted in a smaller slump compared with RAC containing RFA. This may be explained by that the surface of RCA is rougher than that of RFA, and the amount of coarse aggregates is larger than that of fine aggregates in the mix proportions. It can also be seen from Table 3 that f_{cu} and E_c of RAC are lower than those of NC, and the higher r results in the lower f_{cu} and E_c. Moreover, under the same r values, f_{cu} and E_c of RAC with RCA are higher than those of RAC with RFA. These results are similar to the findings presented in [9].

The experiments were not only to obtain the bearing capacity and stiffness of RACFSST stub columns and beams, but also to investigate the failure process up to and beyond the bearing capacity.

2.2. Stub column tests

Fourteen stub columns subjected to concentric compression were tested, as listed in Table 1. The height of stub columns was set to be three times of the outside diameter (circular specimens) or width (square specimens) to avoid the influence of overall buckling and end conditions.

The experiments were carried out on a 3000 kN capacity testing machine. The specimens were placed between the upper and lower platen of the testing machine and the axially compressive loads were applied on the specimens through the rise of the lower platen. The test set-up of stub columns is shown in Fig. 3. Before the tests conducted, the vertical adjustment of specimens was performed to avoid any initial eccentricity. Four positions with the interval of 90° at the mid-height section were selected to paste the strain gauges, and each position had a longitudinal strain gauge and a transverse strain gauge. Two displacement transducers (DTs) were used to measure the axial deformations, as shown in Fig. 3.

It was found that all stub specimens had good deformation-resistant ability and post-peak load-bearing capacity, and the tests were performed in a smooth and controlled fashion. In general, the r had little influence on the failure pattern up to and beyond the bearing capacity of the specimens. However, due to the worse confinement of square tube to core concrete compared with circular one, the stainless steel tube of square specimens had more buckling positions and resulted in a larger peak deformation at the buckling sites. The failure pattern of the stub specimens is shown in Fig. 4.

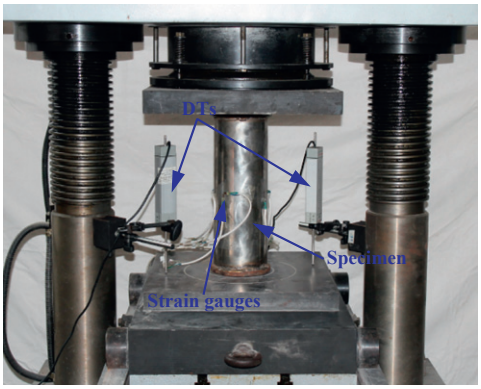

Fig. 3. Test set-up of stub columns.

Fig. 5 illustrates the typical failure pattern of core concrete in stub specimens. It can be seen that core concrete of circular specimens has a good integrity and the thin and dense inclined cracks cover the range of central one-third height. However, for square specimens, core concrete is crushed at the buckling positions of stainless steel tube and the fragments drop off after tube removed. Generally, there is no crack outside the crushing zone of square specimens. This can also be explained by that the confinement to core concrete of square stainless steel tube is worse than that of circular stainless steel tube.

The measured axial load (N) versus strain (ε) curves of the stub specimens are shown in Fig. 6, where the tensile and compressive strains are considered as positive and negative, respectively, and ε_y is the measured yield strain of stainless steel. The experimental bearing capacity (N_{ue}) of the tested specimens is listed in Table 1. It can be seen that, similar to the corresponding CFSST specimens, RACFSST stub columns have the stable N–ε responses and the good deformation-resistant ability. For circular specimens, the strains corresponding to N_{ue} are higher than ε_y; however, the strains corresponding to N_{ue} of square specimens are lower than ε_y. This is similar to the findings of RAC filled carbon steel tube [10], and is produced by the better confinement to core concrete of circular stainless steel tube than square stainless steel tube under the same parametric conditions. It can also be seen from Fig. 6 that, after the axial load reduced to the minimum value, the axial load versus compressive strain curves generally have the stable strengthening behaviour due to the strengthening effect of stainless steel after reaching the yield strength (see Fig. 2).

2.3. Beam tests

A total of 14 beam specimens, including 12 RACFSST beams and two corresponding CFSST beams, were experimentally

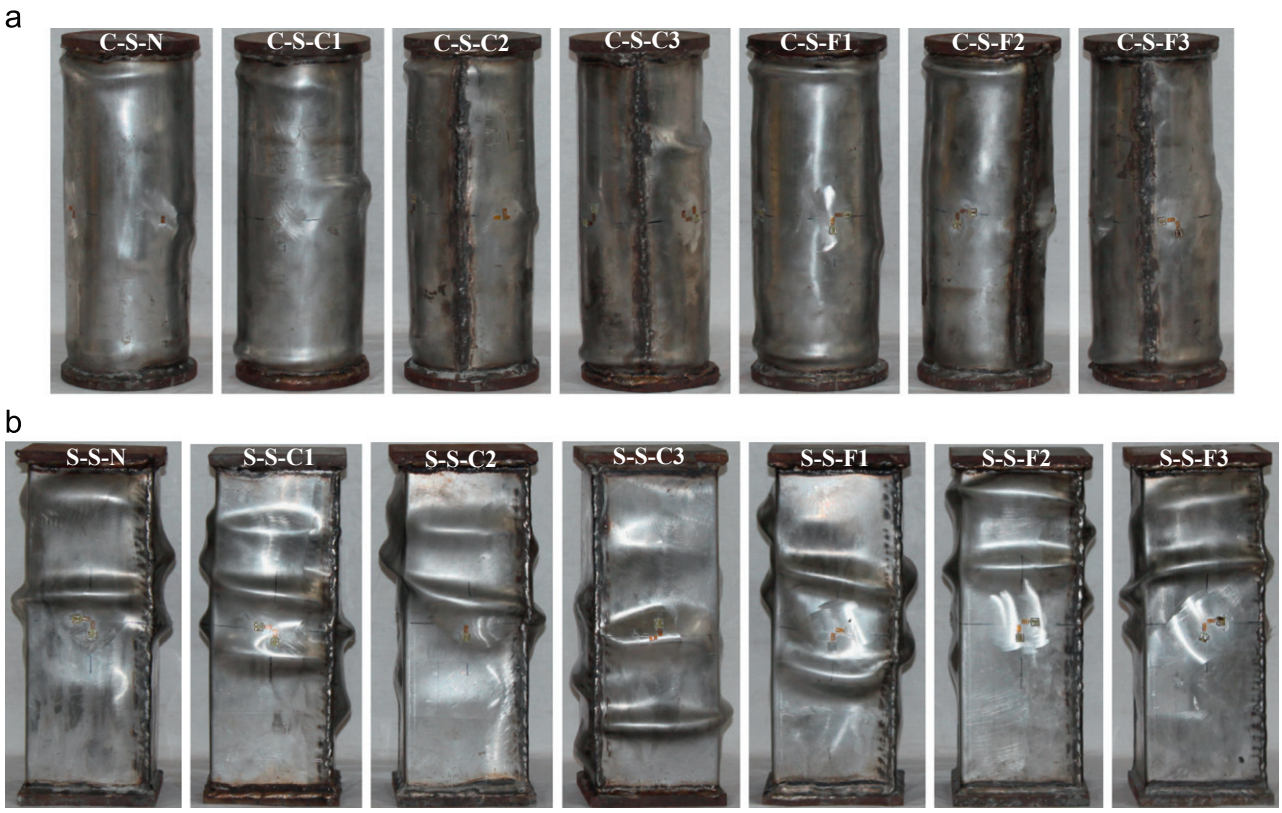

Fig. 4. Failure pattern of the stub specimens. (a) Circular section. (b) Square section.

Fig. 5. Typical failure pattern of core concrete in stub specimens. (a) Circular section. (b) Square section.

investigated. The information of the beam specimens is presented in Table 2. The length of the beam specimens is 1200 mm.

A four-point bending system was used to apply the moment on the beam with pin–pin boundary conditions, and the test set-up and instruments of the beam specimens are shown in Fig. 7. The in-plane vertical displacements at three quartile points and two supports were measured by five DTs. Same as the stub specimen, eight strain gauges (SGs) were used for each beam

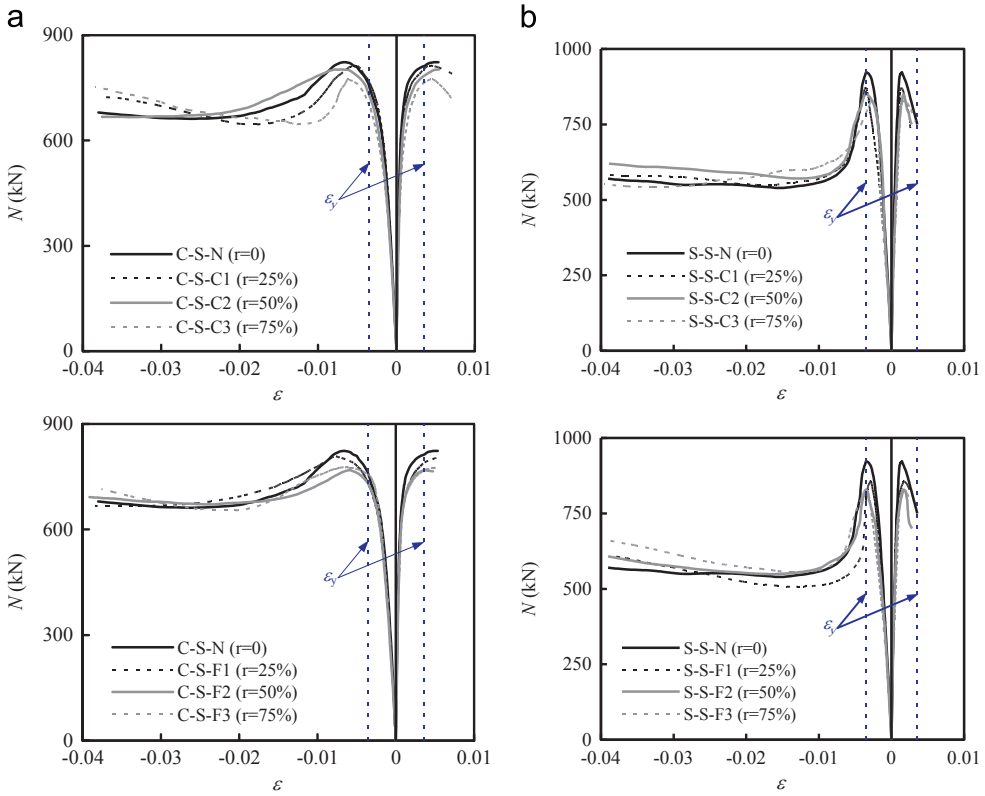

Fig. 6. Axial load (N) versus strain (ε) curves of the stub specimens. (a) Circular section. (b) Square section.

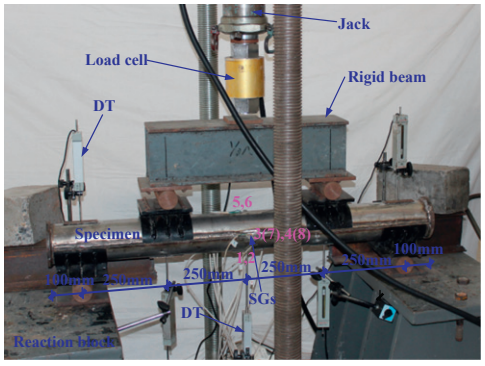

Fig. 7. Test set-up and instruments of the beam specimens.

specimen to obtain the longitudinal and transverse strains at the mid-span section.

Fig. 8 shows the failure pattern of the beam specimens. It can be seen that RACFSST beams have the similar failure pattern as the corresponding CFSST beam specimens, and the r has little effect on the failure pattern of RACFSST beams. Moreover, all beam specimens fail in a very ductile manner and no tensile fracture is observed at the tension area. It can also be found from Fig. 8 that the final failure pattern of the stainless steel tube involves several buckling positions at the compression area and the buckles are distributed equally and symmetrically. However, owing to the better confinement to core concrete of circular stainless steel tube, the peak deformation at the buckling locations of circular specimens is smaller than that of square specimens.

The typical failure pattern of core concrete in beams are shown in Fig. 9. It can be seen that the crushing at the buckling positions of stainless steel tube and the cracking at the tension area happen for core concrete of all specimens. However, due to the worse confinement to core concrete of square stainless steel tube, the crushing of core concrete in square specimens is more evident than that in circular specimens, and the tensile cracks of square specimens are wider than those of circular specimens.

The measured bending moment (M) versus mid-span deflection (u_m) relation of the beam specimens are illustrated in Fig. 10. The M–u_m diagrams show that, similar to concrete filled carbon steel tube [22], there is an initial elastic response, then inelastic behaviour with gradually decreasing stiffness, and finally a evident hardening stage appears after achieving the bending moment capacity. Fig. 11 shows the moment (M) versus extreme fibre strain (ε) relations at mid-span section of the tested beams, where the tensile and compressive strains are considered as positive and negative, respectively. It can be found that, in general, the moment versus longitudinal strain (ε_1 or ε_5) curves tend to stabilise after ε_1 reaching 0.01. As a result, similar to concrete filled carbon steel tube [22], the moment corresponding to the extreme fibre tensile strain (ε_1) of 0.01 is temporarily defined as the bending moment capacity (M_{ue}) of the beam specimens for practical consideration. The M_{ue} of the beam specimens is given in Table 2.

Fig. 12 shows the typical strain distributions at the mid-span section of RACFSST beams, where $m(=M/M_{ue})$ is defined as the bending moment ratio and x represents the position of longitudinal strain gauges at the mid-span section. It can be seen that the linear distribution is generally achieved before and after reaching M_{ue}. This means that the plane section assumption may be suitable for RACFSST beams.

Because of the concrete infill, the beam specimens behaved in a relatively ductile manner and the testing proceeded in a smooth and controlled way. During the tests, the vertical deflections (u) at three quartile points and two supports were approximately in the shape of the half sine wave. Specimens C-B-C2, C-B-F2, S-B-C2 and S-B-F2 were selected to demonstrate the vertical deflection developments of RACFSST beams with different m values, as shown in Fig. 13, where y is the distance away from the left

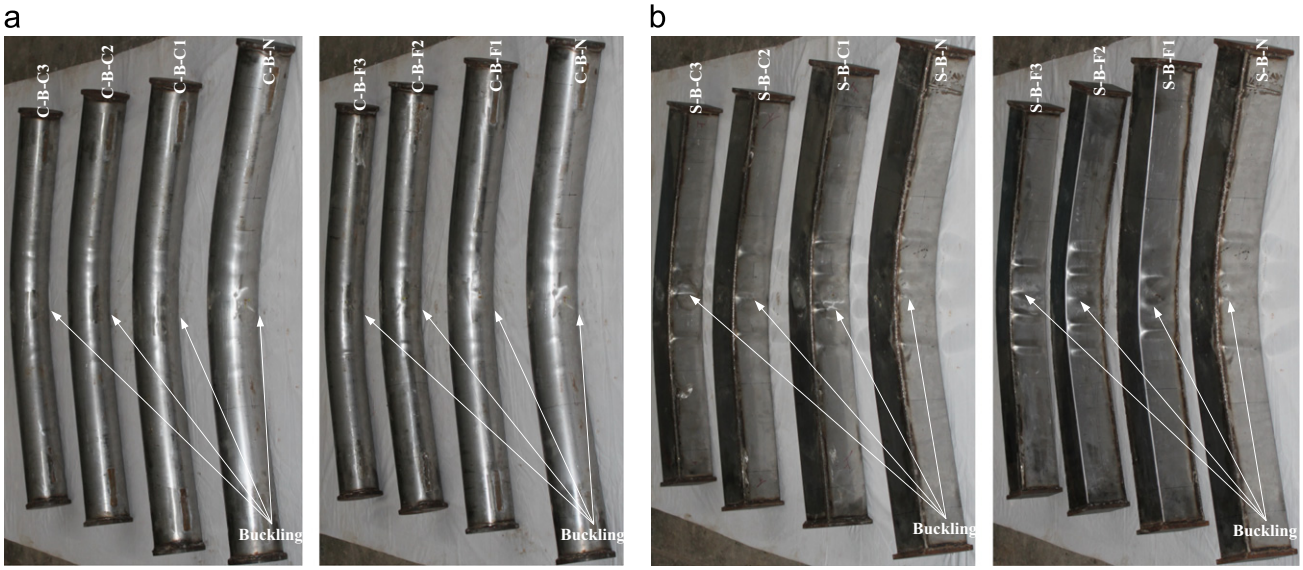

Fig. 8. Failure pattern of the beam specimens. (a) Circular section. (b) Square section.

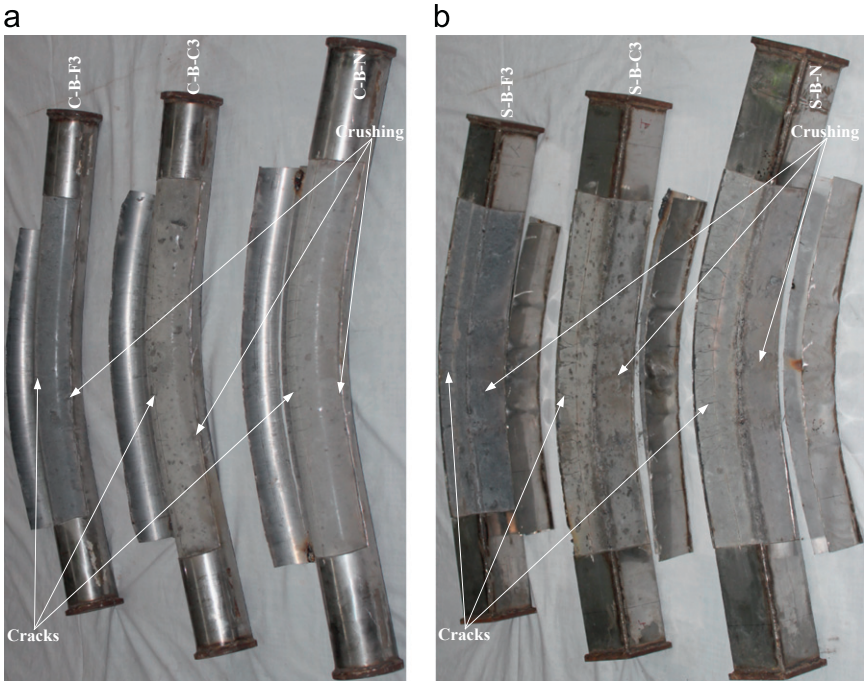

Fig. 9. Typical failure pattern of core concrete in beams. (a) Circular section. (b) Square section.

support in Fig. 7, and the dashed lines are the half sine curve with the same mid-span deflections as the tested results. It is shown that the measured vertical deflection curves are in good agreement with the half sine curves.

The curvatures of the composite beam can be obtained based on the half sine curve assumption [22]. Fig. 14 shows the moment (M) versus curvature (ϕ) relation of the beam specimens. It can be found that, similar to the experimental results of concrete filled carbon steel tube in [22], the M–ϕ curve generally goes into an inelastic stage at 20% of M_{ue} and the initial section flexural stiffness (K_{ie}) can be defined as the secant stiffness corresponding to a moment of $0.2M_{ue}$. Furthermore, the M–ϕ response can also be used to obtain the serviceability-level section flexural stiffness (K_{se}) of the beam specimens, and K_{se} is defined as the secant stiffness corresponding to the serviceability-level moment of $0.6M_{ue}$ [22]. The K_{ie} and K_{se} of the beam specimens are presented in Table 2.

3. Analysis of test results and discussion

3.1. Stub columns

For composite stub columns, the elastic modulus (E_{sc}) is defined as the secant modulus while axial load equal to 40% of N_{ue}, and the E_{sc} of the stub specimens is listed in Table 1. For convenience of analysis, the elastic modulus reduction factor

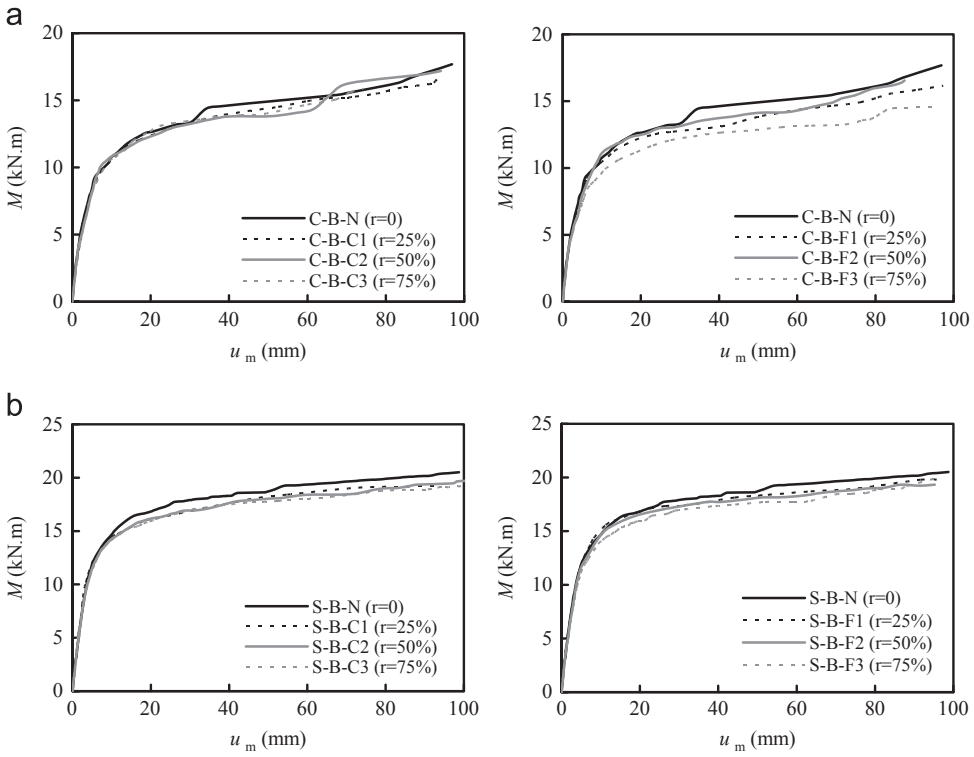

Fig. 10. Moment (M) versus mid-span deflection (u_m) relation of the beam specimens. (a) Circular section. (b) Square section.

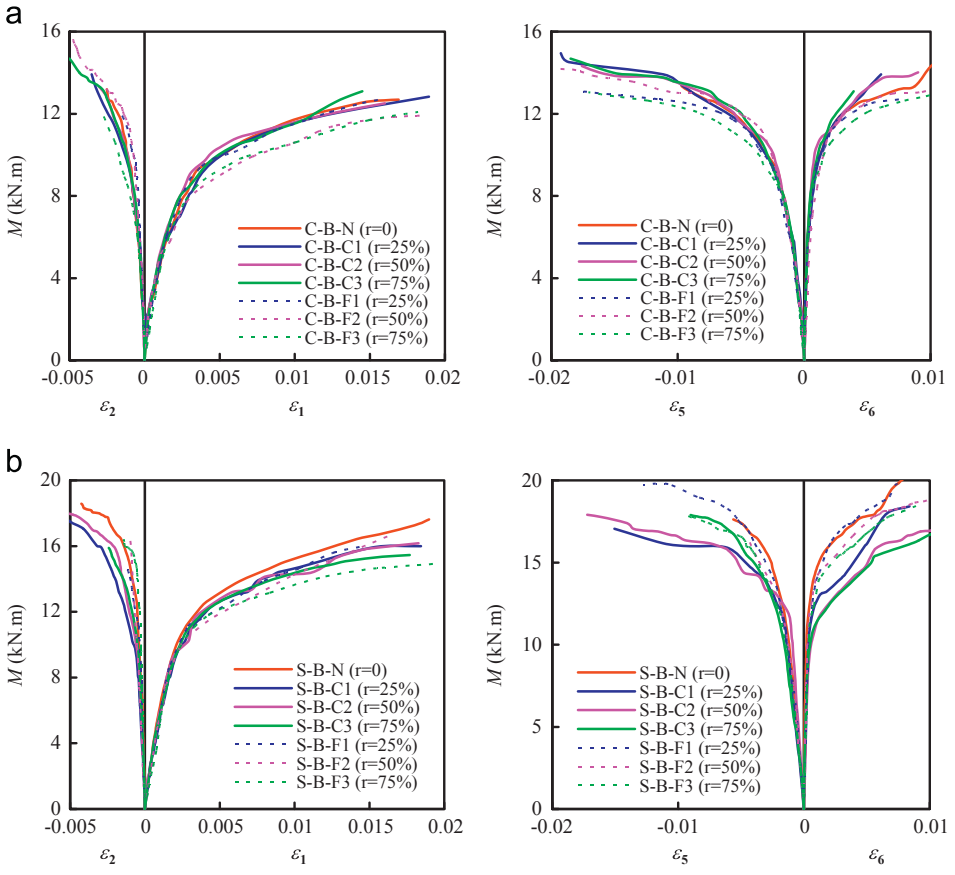

Fig. 11. Moment versus extreme fibre strain relations at the mid-span section. (a) Circular section. (b) Square section.

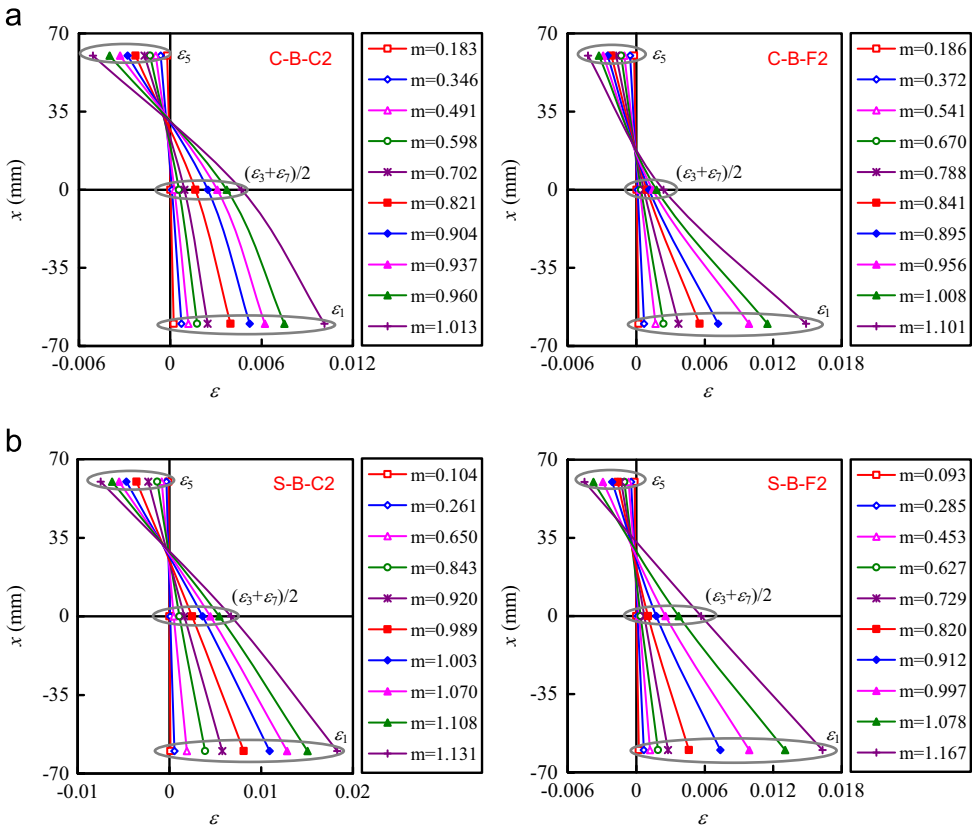

Fig. 12. Typical strain distributions at the mid-span section. (a) Circular section. (b) Square section.

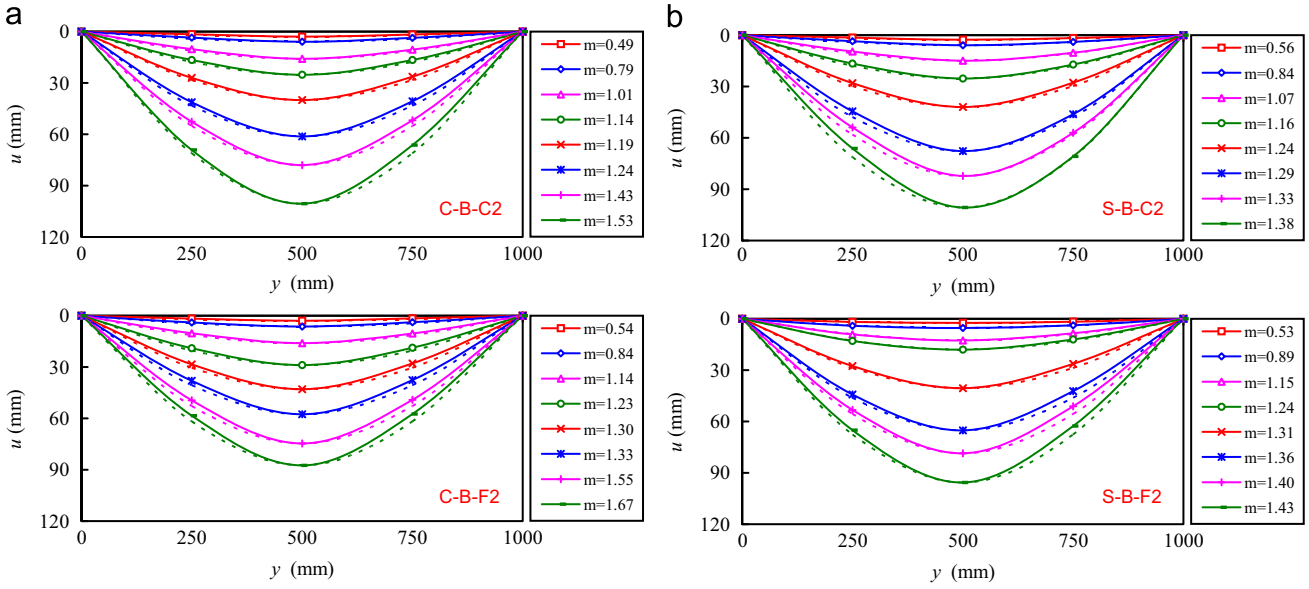

Fig. 13. Typical deflection curves along the span of the beam specimens. (a) Circular section. (b) Square section.

(ERF) and the bearing capacity reduction factor (BRF) of the stub specimens are defined as

$$ERF = \frac{E_{sc,R} - E_{sc,N}}{E_{sc,N}} \tag{1}$$

$$BRF = \frac{N_{ue,R} - N_{ue,N}}{N_{ue,N}} \tag{2}$$

where $E_{sc,R}$ ($N_{ue,R}$) and $E_{sc,N}$ ($N_{ue,N}$) are the elastic modulus (bearing capacity) of RACFSST specimens and the corresponding CFSST specimens. The calculated ERF and BRF of the stub specimens are given in Table 1.

The effect of r on E_{sc} and ERF of the stub specimens is shown in Fig. 15, where the ERF of plain concrete, which can be obtained by replacing E_{sc} of composite specimens in Eq. (1) by E_c of RAC and the corresponding NC, is shown in dashed lines. It can be seen from Fig. 15 and Table 1 that, in general, E_{sc} and ERF of RACFSST

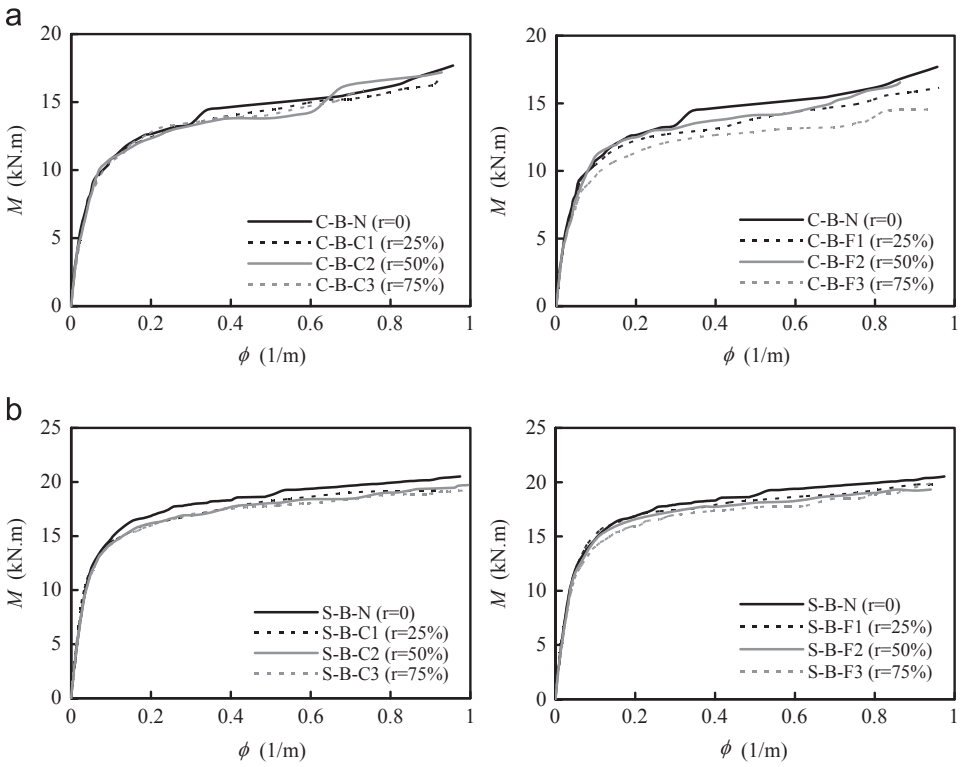

Fig. 14. Moment (M) versus curvature (ϕ) relation of the beam specimens. (a) Circular section. (b) Square section.

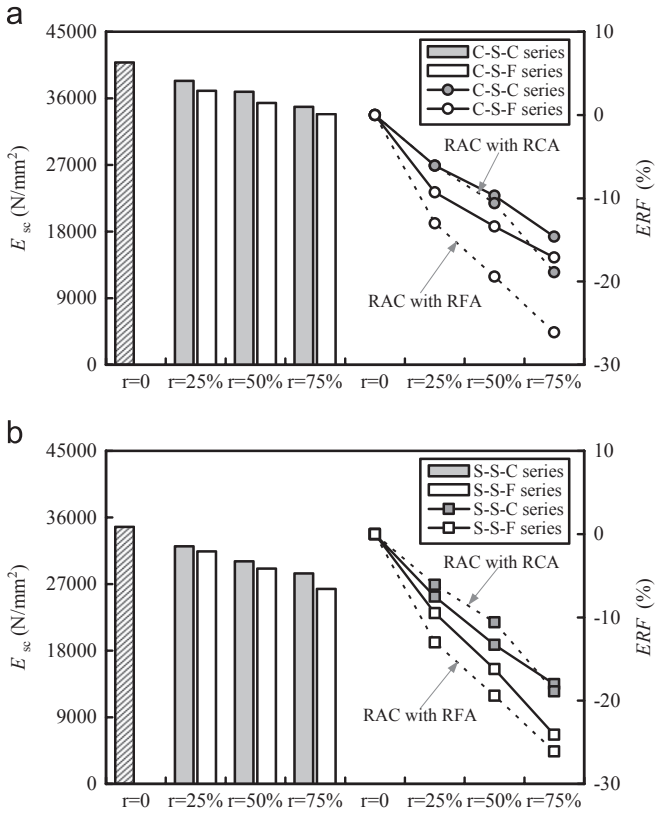

Fig. 15. Effect of r on E_{sc} and ERF of the stub specimens. (a) Circular section. (b) Square section.

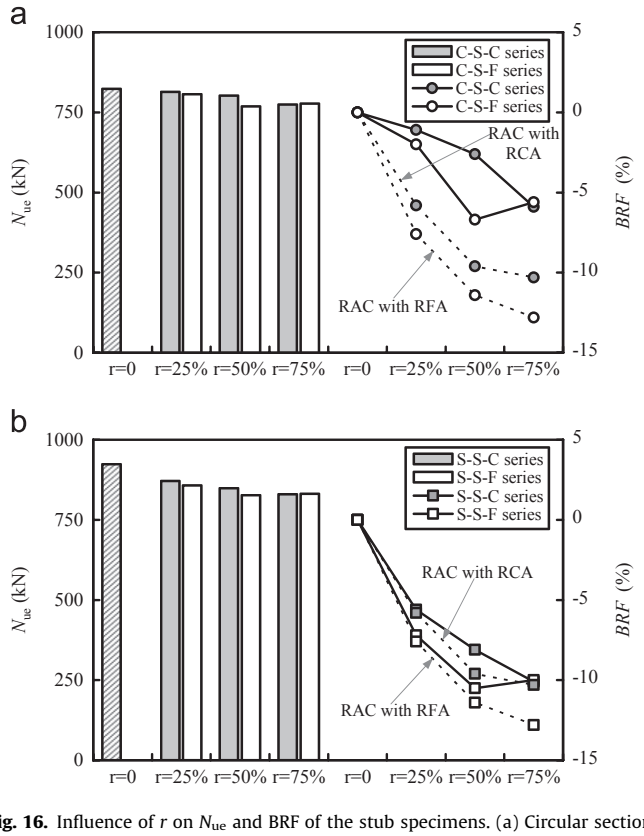

Fig. 16. Influence of r on N_{ue} and BRF of the stub specimens. (a) Circular section. (b) Square section.

specimens are lower than those of the corresponding CFSST specimens, and the higher r results in the lower E_{sc} and ERF. The E_{sc} of RACFSST specimens with RCA and RFA is 6.1–18.0% and 9.3–24.1% lower than that of CFSST specimens, respectively. Under the same r value, the specimens containing RCA have the higher E_{sc} and ERF compared with the specimens containing RFA. These phenomena are mainly determined by the changing rules of E_c. Furthermore,

Table 4
Comparison of N_{uc} and N_{ue} of the stub specimens.

No.	Specimen	N_{ue} (kN)	ACI 318-05		AIJ		ANSI/AISC 360-05		BS 5400-5		DB21/T1746-2009		EC4	
			N_{uc} (kN)	$\frac{N_{uc}}{N_{ue}}$	N_{uc} (kN)	$\frac{N_{uc}}{N_{ue}}$	N_{uc} (kN)	$\frac{N_{uc}}{N_{ue}}$	N_{uc} (kN)	$\frac{N_{uc}}{N_{ue}}$	N_{uc} (kN)	$\frac{N_{uc}}{N_{ue}}$	N_{uc} (kN)	$\frac{N_{uc}}{N_{ue}}$
1	C−S−N	823.2	644.7	0.783	695.6	0.845	692.4	0.841	578.5	0.703	720.1	0.875	805.8	0.979
2	C−S−C1	813.8	617.9	0.759	668.8	0.822	662.9	0.815	564.3	0.693	693.2	0.852	775.7	0.953
3	C−S−C2	802.2	600.5	0.749	651.1	0.812	643.3	0.802	555.1	0.692	675.4	0.842	755.7	0.942
4	C−S−C3	774.3	597.6	0.772	648.2	0.837	640.1	0.827	553.6	0.715	672.5	0.869	752.5	0.972
5	C−S−F1	806.7	609.9	0.756	660.7	0.819	654.0	0.811	560.1	0.694	685.1	0.849	766.6	0.950
6	C−S−F2	768.4	592.6	0.771	643.0	0.837	634.4	0.826	550.9	0.717	667.3	0.868	746.6	0.972
7	C−S−F3	777.2	586.0	0.754	636.3	0.819	627.1	0.807	547.4	0.704	660.6	0.850	739.2	0.951
Mean value				0.763		0.827		0.818		0.703		0.858		**0.960**
Standard deviation				0.012		0.012		0.014		0.010		0.012		**0.014**
1	S−S−N	923.4	820.9	0.889	820.9	0.889	816.0	0.884	590.4	0.639	851.7	0.922	923.4	1.000
2	S−S−C1	871.5	786.8	0.903	786.8	0.903	782.2	0.898	572.4	0.657	817.0	0.937	883.2	1.013
3	S−S−C2	848.5	764.6	0.901	764.6	0.901	759.8	0.895	560.7	0.661	793.9	0.936	856.7	1.010
4	S−S−C3	830.0	760.9	0.917	760.9	0.917	756.2	0.911	558.7	0.673	790.1	0.952	852.3	1.027
5	S−S−F1	857.1	776.6	0.906	776.6	0.906	772.0	0.901	567.0	0.662	806.5	0.941	871.1	1.016
6	S−S−F2	826.9	754.5	0.912	754.5	0.912	749.6	0.907	555.3	0.672	783.4	0.947	844.5	1.021
7	S−S−F3	831.1	746.2	0.898	746.2	0.898	741.3	0.892	550.9	0.663	774.7	0.932	834.6	1.004
Mean value				0.904		0.904		0.898		0.661		**0.938**		1.013
Standard deviation				0.009		0.009		0.009		0.011		**0.010**		0.009

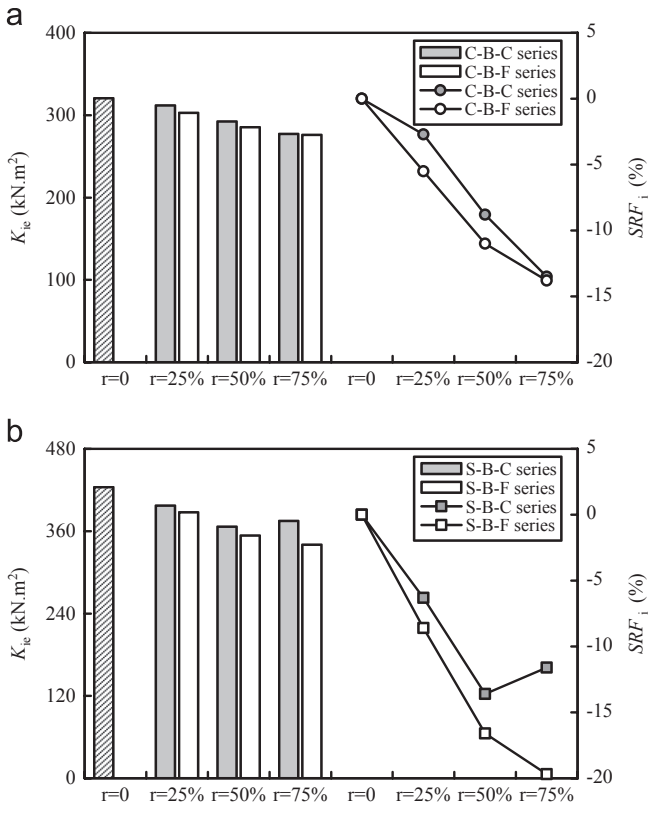

Fig. 17. Influence of r on K_{ie} and SRF_i of the beam specimens. (a) Circular section. (b) Square section.

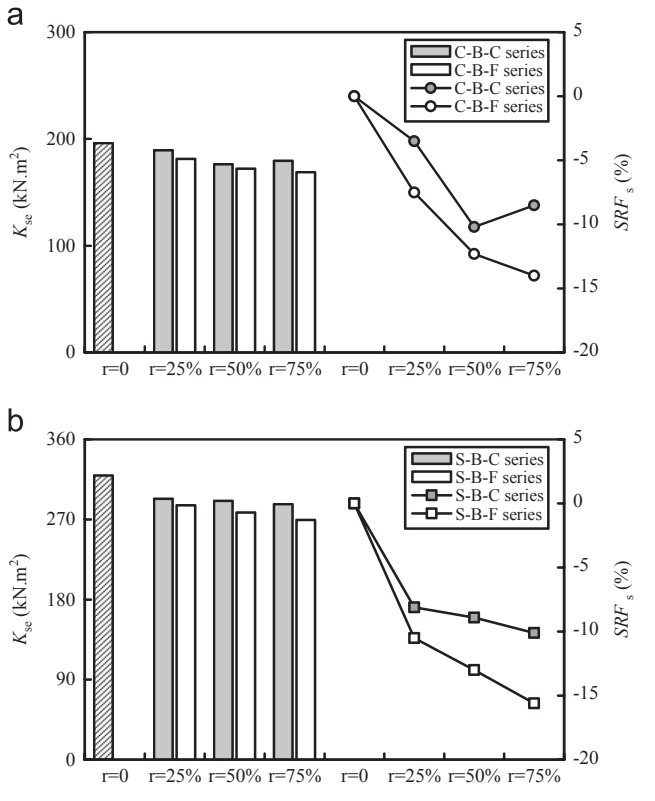

Fig. 18. Influence of r on K_{se} and SRF_s of the beam specimens. (a) Circular section. (b) Square section.

owing to the better confinement to core concrete of circular stainless steel tube, E_{sc} and ERF of circular specimens are higher than those of square specimens. It can also be found from Fig. 15 that, except for square specimens with RAC containing 25% and 50% RFA (Specimens S-S-F1 and S-S-F2), ERF of RAC is lower than that of the corresponding RACFSST specimens. This indicates that, in general, the deformation-resistant ability of core RAC is improved due to the confinement of the outer stainless steel tube.

Fig. 16 illustrates the influence of r on N_{ue} and BRF of the stub specimens, where the similar BRF of plain concrete obtained by $(f_{cu,test,N}-f_{cu,test,R})/f_{cu,test,N}$ is shown in dashed lines, in which $f_{cu,test,R}$ and $f_{cu,test,N}$ are the cube compressive strength of RAC and the corresponding NC while the tests conducted. It can be seen from Fig. 16 and Table 1 that, in general, N_{ue} and BRF of RACFSST specimens are lower than those of the corresponding CFSST specimens, and the higher r leads to the lower N_{ue} and BRF. The N_{ue} of CFSST specimens is 1.1–10.1% and 2.0–10.5% higher

than that of RACFSST specimens with RCA and RFA, respectively. Under the same r value, the specimens containing RCA have the higher BRF compared with the specimens containing RFA. These phenomena are mainly caused by the differences of the compressive strength of concrete. Moreover, due to the worse confinement to core concrete of square stainless steel tube, BRF of square specimens are lower than those of circular specimens. It can also be found from Fig. 16 that, BRF of RAC is lower than that of the corresponding RACFSST specimens. This means that, owing to the confinement of stainless steel tube, the compressive strength of RAC can be evidently enhanced.

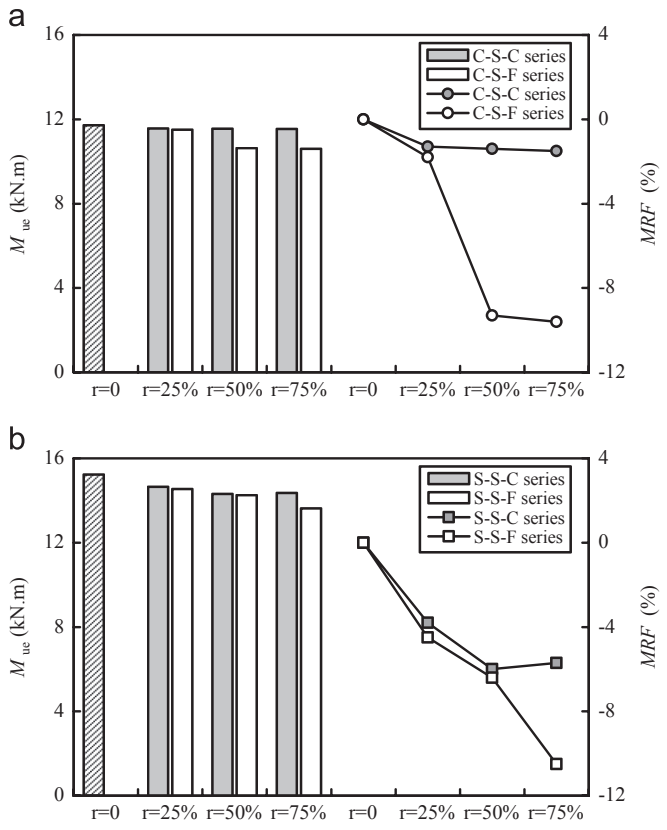

Fig. 19. Effect of r on M_{ue} and MRF of the beam specimens. (a) Circular section. (b) Square section.

To date, there is no design recommendation related to the bearing capacity of RACFSST stub column. In this paper, the formulae in design codes for concrete filled carbon steel tube are temporarily used for predicting the bearing capacity of RACFSST stub columns and the corresponding CFSST stub columns. In all calculations, the material partial safety factors are set to unity, and the measured yield strength of stainless steel and cube compressive strength of concrete while the tests carried out are adopted.

The calculated bearing capacity of the stub columns (N_{uc}) using the design equations in ACI 318-05 [16], AIJ [17], ANSI/AISC 360-05 [18], BS 5400-5 [19], DB21/T1746-2009 [20] and EC4 [21] are compared with the experimental results (N_{ue}). The comparison between N_{uc} and N_{ue} of the stub specimens is presented in Table 4. It can be seen that, except for the results of square specimens predicted by EC4, the calculated bearing capacities using the aforementioned design codes are conservative. For circular specimens, DB21/T1746-2009, AIJ, ANSI/AISC 360-05, ACI 318-05 and BS 5400-5 give the bearing capacity about 14%, 17%, 18%, 24% and 30% lower than the results obtained in the tests, respectively, and overall EC4 with a mean value of 0.960 and a standard deviation of 0.014 is the best predictor. For square specimens, EC4 gives a slight higher prediction, and ACI 318-05, AIJ and ANSI/AISC 360-05 give the bearing capacity about 10% lower than the experimental results. Overall, DB21/T1746-2009 with a mean value of 0.938 and a standard deviation of 0.010 is the best predictor, and BS 5400-5 with a mean value of 0.661 and a standard deviation of 0.011 is the most conservative predictor.

3.2. Beams

To account for the influence of r on the flexural stiffness and bending moment capacity of RACFSST beams, the flexural stiffness reduction factor (SRF_i and SRF_s) and bending moment capacity reduction factor (MRF) are defined as

$$SRF_i = \frac{K_{ie,R} - K_{ie,N}}{K_{ie,N}} \tag{3}$$

$$SRF_s = \frac{K_{se,R} - K_{se,N}}{K_{se,N}} \tag{4}$$

Table 5
Comparison of K_{ic} and K_{ie} of the beam specimens.

No.	Specimen	K_{ie} (kN.m^2)	ACI 318-05		AIJ		ANSI/AISC 360-05		BS 5400-5		DB21/T1746-2009		EC4	
			K_{ic} (kN.m^2)	$\frac{K_{ic}}{K_{ie}}$	K_{ic} (kN.m^2)	$\frac{K_{ic}}{K_{ie}}$	K_{ic} (kN.m^2)	$\frac{K_{ic}}{K_{ie}}$	K_{ic} (kN.m^2)	$\frac{K_{ic}}{K_{ie}}$	K_{ic} (kN.m^2)	$\frac{K_{ic}}{K_{ie}}$	K_{ic} (kN.m^2)	$\frac{K_{ic}}{K_{ie}}$
1	C–B–N	320.5	287.2	0.896	294.4	0.919	451.2	1.408	387.2	1.208	492.6	1.537	429.3	1.339
2	C–B–C1	311.8	285.5	0.916	292.6	0.938	444.6	1.426	379.8	1.218	489.7	1.571	425.9	1.366
3	C–B–C2	292.3	284.2	0.972	291.4	0.997	439.8	1.505	374.7	1.282	487.6	1.668	423.4	1.449
4	C–B–C3	277.1	283.7	1.024	290.9	1.050	438.0	1.581	372.8	1.345	486.8	1.757	422.5	1.525
5	C–B–F1	302.8	284.8	0.941	292.0	0.964	442.1	1.460	377.1	1.245	488.6	1.614	424.6	1.402
6	C–B–F2	285.3	282.9	0.992	290.1	1.017	434.9	1.524	369.5	1.295	485.3	1.701	420.9	1.475
7	C–B–F3	276.2	282.5	1.023	289.6	1.049	433.1	1.568	367.6	1.331	484.5	1.754	419.9	1.520
Mean value				0.966		**0.990**		1.496		1.275		1.657		1.439
Standard deviation				0.051		**0.052**		0.067		0.053		0.087		0.073
1	S–B–N	424.0	487.5	1.150	499.7	1.179	766.1	1.807	657.3	1.550	727.6	1.716	728.8	1.719
2	S–B–C1	397.2	484.6	1.220	496.8	1.251	754.8	1.900	644.8	1.623	724.0	1.823	723.1	1.820
3	S–B–C2	366.5	482.5	1.317	494.7	1.350	746.6	2.037	636.0	1.735	721.3	1.968	718.8	1.961
4	S–B–C3	374.9	481.7	1.285	493.9	1.317	743.6	1.983	632.8	1.688	720.2	1.921	717.2	1.913
5	S–B–F1	387.6	483.5	1.247	495.7	1.279	750.5	1.936	640.2	1.652	722.6	1.864	720.8	1.860
6	S–B–F2	353.7	480.3	1.358	492.5	1.392	738.3	2.087	627.3	1.774	718.4	2.031	714.5	2.020
7	S–B–F3	340.4	479.5	1.409	491.7	1.444	735.2	2.160	624.0	1.833	717.3	2.107	712.8	2.094
Mean value				**1.284**		1.316		1.987		1.694		1.919		1.912
Standard deviation				**0.087**		0.089		0.119		0.096		0.132		0.126

$$MRF = \frac{M_{ue,R} - M_{ue,N}}{M_{ue,N}} \quad (5)$$

where $K_{ie,R}$($K_{se,R}$) and $M_{ue,R}$ are the initial (serviceability-level) section flexural stiffness and bending moment capacity of RACFSST beam specimens, and $K_{ie,N}$($K_{se,N}$) and $M_{ue,N}$ are the initial (serviceability-level) section flexural stiffness and bending moment capacity of the corresponding CFSST beam specimens, respectively. The calculated SRF_i, SRF_s and MRF are listed in Table 2.

Figs. 17 and 18 show the influence of r on flexural stiffness (K_{ie} and K_{se}) and flexural stiffness reduction factor (SRF_i and SRF_s) of the beam specimens. It can be seen from Figs. 17 and 18 and Table 2 that, K_{ie} (K_{se}) and SRF_i (SRF_s) of RACFSST beam specimens are lower than those of the corresponding CFSST specimens, and the higher r also results in the lower K_{ie} (K_{se}) and SRF_i (SRF_s). The K_{ie} (K_{se}) of RACFSST specimens with RCA and RFA is 2.7–13.6% (3.5–10.2%) and 5.5–19.7% (7.5–15.6%) lower than that of CFSST specimens, respectively. Under the same r value, the specimens with RCA have the higher K_{ie} (K_{se}) and SRF_i (SRF_s) compared with the specimens with RFA. These phenomena are mainly determined by the variation rules of E_c. Furthermore, owing to the worse confinement to core concrete of square stainless steel tube, SRF_i (SRF_s) of square specimens are lower than those of circular specimens.

The effect of r on M_{ue} and MRF of the beam specimens is illustrated in Fig. 19. It can be seen from Fig. 19 and Table 2 that, M_{ue} and MRF of RACFSST beam specimens are lower than those of the corresponding CFSST beam specimens, and the higher r results in the lower M_{ue} and MRF. The M_{ue} of RACFSST specimens with RCA and RFA is 1.3–6.0% and 1.8–10.5% lower than that of CFSST specimens, respectively. Under the same r value, the specimens with RCA have the higher M_{ue} and MRF compared with the specimens with RFA. The lowering in bending moment

Table 6
Comparison of K_{sc} and K_{se} of the beam specimens.

No.	Specimen	K_{se} (kN.m^2)	ACI 318-05		AIJ		ANSI/AISC 360-05		BS 5400-5		DB21/T1746-2009		EC4	
			K_{sc} (kN.m^2)	$\frac{K_{sc}}{K_{se}}$	K_{sc} (kN.m^2)	$\frac{K_{sc}}{K_{se}}$	K_{sc} (kN.m^2)	$\frac{K_{sc}}{K_{se}}$	K_{sc} (kN.m^2)	$\frac{K_{sc}}{K_{se}}$	K_{sc} (kN.m^2)	$\frac{K_{sc}}{K_{se}}$	K_{sc} (kN.m^2)	$\frac{K_{sc}}{K_{se}}$
1	C–B–N	196.2	287.2	1.464	294.4	1.501	451.2	2.300	387.2	1.973	492.6	2.511	429.3	2.188
2	C–B–C1	189.3	285.5	1.508	292.6	1.546	444.6	2.349	379.8	2.006	489.7	2.587	425.9	2.250
3	C–B–C2	176.2	284.2	1.613	291.4	1.654	439.8	2.496	374.7	2.127	487.6	2.767	423.4	2.403
4	C–B–C3	179.5	283.7	1.581	290.9	1.621	438.0	2.440	372.8	2.077	486.8	2.712	422.5	2.354
5	C–B–F1	181.4	284.8	1.570	292.0	1.610	442.1	2.437	377.1	2.079	488.6	2.693	424.6	2.341
6	C–B–F2	172.1	282.9	1.644	290.1	1.686	434.9	2.527	369.5	2.147	485.3	2.820	420.9	2.446
7	C–B–F3	168.8	282.5	1.674	289.6	1.716	433.1	2.566	367.6	2.178	484.5	2.870	419.9	2.488
Mean value				**1.579**		1.619		2.445		2.084		2.709		2.353
Standard deviation				**0.074**		0.076		0.095		0.074		0.127		0.106
1	S–B–N	319.3	487.5	1.527	499.7	1.565	766.1	2.399	657.3	2.059	727.6	2.279	728.8	2.282
2	S–B–C1	293.3	484.6	1.652	496.8	1.694	754.8	2.573	644.8	2.198	724.0	2.468	723.1	2.465
3	S–B–C2	290.8	482.5	1.659	494.7	1.701	746.6	2.567	636.0	2.187	721.3	2.480	718.8	2.472
4	S–B–C3	287.2	481.7	1.677	493.9	1.720	743.6	2.589	632.8	2.203	720.2	2.508	717.2	2.497
5	S–B–F1	285.8	483.5	1.692	495.7	1.734	750.5	2.626	640.2	2.240	722.6	2.528	720.8	2.522
6	S–B–F2	277.9	480.3	1.728	492.5	1.772	738.3	2.657	627.3	2.257	718.4	2.585	714.5	2.571
7	S–B–F3	269.4	479.5	1.780	491.7	1.825	735.2	2.729	624.0	2.316	717.3	2.663	712.8	2.646
Mean value				**1.674**		1.716		2.592		2.209		2.502		2.494
Standard deviation				**0.078**		0.081		0.102		0.080		0.119		0.112

Table 7
Comparison of M_{uc} and M_{ue} of the beam specimens.

No.	Specimen	M_{ue} (kN.m)	ACI 318-05		AIJ		ANSI/AISC 360-05		BS 5400-5		DB21/T1746-2009		EC4	
			M_{uc} (kN.m)	$\frac{M_{uc}}{M_{ue}}$	M_{uc} (kN.m)	$\frac{M_{uc}}{M_{ue}}$	M_{uc} (kN.m)	$\frac{M_{uc}}{M_{ue}}$	M_{uc} (kN.m)	$\frac{M_{uc}}{M_{ue}}$	M_{uc} (kN.m)	$\frac{M_{uc}}{M_{ue}}$	M_{uc} (kN.m)	$\frac{M_{uc}}{M_{ue}}$
1	C–B–N	11.72	9.43	0.805	7.09	0.605	7.09	0.605	8.46	0.722	8.73	0.745	9.17	0.782
2	C–B–C1	11.57	9.41	0.813	7.09	0.613	7.09	0.613	8.41	0.727	8.62	0.745	9.11	0.787
3	C–B–C2	11.56	9.39	0.812	7.09	0.613	7.09	0.613	8.38	0.725	8.55	0.740	9.08	0.785
4	C–B–C3	11.54	9.39	0.814	7.09	0.614	7.09	0.614	8.37	0.725	8.53	0.739	9.07	0.786
5	C–B–F1	11.51	9.40	0.817	7.09	0.616	7.09	0.616	8.39	0.729	8.59	0.746	9.10	0.791
6	C–B–F2	10.63	9.38	0.882	7.09	0.667	7.09	0.667	8.36	0.786	8.51	0.801	9.06	0.852
7	C–B–F3	10.60	9.38	0.885	7.09	0.669	7.09	0.669	8.36	0.789	8.48	0.800	9.05	0.854
Mean value				**0.833**		0.628		0.628		0.743		0.759		0.805
Standard deviation				**0.035**		0.027		0.027		0.030		0.028		0.033
1	S–B–N	15.23	13.34	0.876	10.64	0.699	10.64	0.699	13.00	0.854	12.70	0.834	13.15	0.863
2	S–B–C1	14.65	13.28	0.906	10.64	0.726	10.64	0.726	12.96	0.885	12.52	0.855	13.11	0.895
3	S–B–C2	14.31	13.23	0.925	10.64	0.744	10.64	0.744	12.92	0.903	12.40	0.867	13.08	0.914
4	S–B–C3	14.36	13.23	0.921	10.64	0.741	10.64	0.741	12.92	0.900	12.38	0.862	13.08	0.911
5	S–B–F1	14.55	13.26	0.911	10.64	0.731	10.64	0.731	12.94	0.889	12.46	0.856	13.10	0.900
6	S–B–F2	14.25	13.21	0.927	10.64	0.747	10.64	0.747	12.91	0.906	12.34	0.866	13.07	0.917
7	S–B–F3	13.63	13.19	0.968	10.64	0.781	10.64	0.781	12.90	0.946	12.30	0.902	13.06	0.958
Mean value				**0.919**		0.738		0.738		0.898		0.863		0.908
Standard deviation				**0.028**		0.025		0.025		0.028		0.021		0.028

capacity of RACFSST beam specimens can also be attributed to the lower cube compressive strength of RAC compared with NC.

The calculated initial section flexural stiffness (K_{ic}), serviceability-level section flexural stiffness (K_{sc}) and bending moment capacity (M_{uc}) of the beam specimens using the aforementioned six design codes are compared with the experimental results in Tables 5–7, respectively. In calculation of the bending moment capacity, the material partial safety factors were also set to unity.

Results in Table 5 show that ANSI/AISC 360-05, BS 5400-5, DB21/T1746-2009 and EC4 give an unsafe prediction for the initial section flexural stiffness of the beam specimens. For circular specimens, DB21/T1746-2009 is the most unsafe one and gives a 66% higher calculated result. ANSI/AISC 360-05, BS 5400-5, and EC4 give the calculated results about 50%, 28% and 44% higher than the experimental results, respectively. Overall, ACI 318-05 and AIJ, which give the calculated results about 3% and 1% lower than the experimental results, respectively, are the best predictors. For square specimens, ANSI/AISC 360-05 is the most unsafe one and nearly gives a twice larger calculated result. Overall, ACI 318-05 gives the closest prediction with a mean value of 1.284 and a standard deviation of 0.087. Results in Table 6 also show that all six design codes give an unsafe prediction for the serviceability-level section flexural stiffness of the beam specimens. In general, K_{sc} of ACI 318-05 is the closest prediction, and the mean value of K_{sc}/K_{se} for circular and square specimens is 1.579 and 1.674, respectively.

It is clearly shown in Table 7 that, all six design codes are conservative for calculating the bending moment capacity of RACFSST beams and the corresponding CFSST beams. For circular specimens, AIJ, ANSI/AISC 360-05, BS 5400-5, DB21/T1746-2009 and EC4 give about 17–37% lower predictions. Overall, ACI 318-05, which gives a mean value of 0.833 and a standard deviation of 0.035, is the best predictor. For square specimens, the calculated results are closer to the experimental results compared with circular specimens. On average, the M_{uc} of AIJ and ANSI/AISC 360-05 are about 26% lower than the experimental results. The calculated results of DB21/T1746-2009, BS 5400-5 and EC4 are about 9–14% lower than the experimental results. Overall, ACI 318-05, which gives a mean of 0.919 and a standard deviation of 0.028, is the best predictor for the bending moment capacity of square CFSST and RACFSST beams.

4. Conclusions

The investigation on the experimental behaviour of RACFSST stub columns and beams under short-term loadings is presented in this paper. Based on the observations and analytical results, the following conclusions can be drawn:

(1) The compressive and flexural behaviour of RACFSST specimens are similar to those of the corresponding CFSST specimens, and RACFSST stub columns and beams also have the stable load versus deformation responses and the good deformation-resistant ability.
(2) Compared with CFSST specimens, the elastic modulus and bearing capacity reduction of RACFSST stub specimens are 6.1–24.1% and 1.1–10.5%, respectively, and the initial section flexural stiffness, serviceability-level section flexural stiffness and bending moment capacity reduction of RACFSST beam specimens are 2.7–19.7%, 3.5–15.6% and 1.3–10.5%, respectively.
(3) In general, the bearing capacity of RACFSST stub columns and beams can be conservatively calculated by the existing design codes for concrete filled carbon steel tube; however, except for the initial section flexural stiffness of circular specimens predicted by ACI 318-05 and AIJ, the calculated flexural stiffness of RACFSST beams are obviously higher than the experimental results.
(4) The performance of core RAC is generally improved owing to the confinement of the outer stainless steel tube.

Acknowledgements

The research reported in this paper is supported by the Science Fund for Creative Research Groups of the National Natural Science Foundation of China (51121005), the Fundamental Research Funds for the Central Universities (DUT12ZD215) and the Independent Research Funds of the State Key Laboratory of Coastal and Offshore Engineering (SL2012-1). The financial support is highly appreciated. The authors also wish to thank Mr. Kai Cao for his assistance in the tests.

References

[1] Uy B. Stability and ductility of high performance steel sections with concrete infill. Journal of Constructional Steel Research 2008;64(7-8):748–54.
[2] Uy B, Tao Z, Han LH. Behaviour of short and slender concrete-filled stainless steel tubular columns. Journal of Constructional Steel Research 2011;67(3):360–78.
[3] Feng R, Young B. Tests of concrete-filled stainless steel tubular T-joints. Journal of Constructional Steel Research 2008;64(11):1283–93.
[4] Feng R, Young B. Behaviour of concrete-filled stainless steel tubular X-joints subjected to compression. Thin-Walled Structures 2009;47(4):365–74.
[5] Feng R, Young B. Design of concrete-filled stainless steel tubular connections. Advances in Structural Engineering 2010;13(3):471–92.
[6] Dai X, Lam D. Axial compressive behaviour of stub concrete-filled columns with elliptical stainless steel hollow sections. Steel and Composite Structures 2010;10(6):517–39.
[7] Lam D, Gardner L, Burdett M. Behaviour of axially loaded concrete filled stainless steel elliptical stub columns. Advances in Structural Engineering 2010;13(3):493–500.
[8] Tao Z, Uy B, Liao FY, Han LH. Nonlinear analysis of concrete-filled square stainless steel stub columns under axial compression. Journal of Constructional Steel Research 2011;67(11):1719–32.
[9] Hansen TC. Recycling of demolished concrete and masonry. In: Hansen TC, editor. Report of RILEM TC 37-DRC on demolition and reuse of concrete. London: E&FN Spon; 1992.
[10] Yang YF, Han LH. Compressive and flexural behaviour of recycled aggregate concrete filled steel tubes (RACFST) under short-term loadings. Steel and Composite Structures 2006;6(3):257–84.
[11] Yang YF, Han LH. Experimental behaviour of recycled aggregate concrete filled steel tubular columns. Journal of Constructional Steel Research 2006;62(12):1310–24.
[12] Yang YF, Han LH, Wu X. Concrete shrinkage and creep in recycled aggregate concrete-filled steel tubes. Advances in Structural Engineering 2008;11(4):383–96.
[13] Yang YF. Behaviour of recycled aggregate concrete-filled steel tubular columns under long-term sustained loads. Advances in Structural Engineering 2011;14(2):189–206.
[14] Yang YF, Han LH, Zhu LT. Experimental performance of recycled aggregate concrete-filled circular steel tubular columns subjected to cyclic flexural loadings. Advances in Structural Engineering 2009;12(2):183–94.
[15] Yang YF, Zhu LT. Recycled aggregate concrete filled steel SHS beam-columns subjected to cyclic loading. Steel and Composite Structures 2009;9(1):s19–38.
[16] ACI 318-05. Building code requirements for structural concrete and commentary. Detroit, USA: Farmington Hills (MI), American Concrete Institute; 2005.
[17] AIJ. Recommendations for design and construction of concrete filled steel tubular structures. Tokyo, Japan: Architectural Institute of Japan; 1997.
[18] ANSI/AISC 360-05. Specification for structural steel buildings. Chicago, USA: American Institute of Steel Construction, Inc.; , 2005.
[19] BS 5400-5. Steel, concrete and composite bridges. Part 5: code of practice for the design of composite bridges. British Standards Institution; 2005.
[20] DB21/T1746-2009. Technical specification for concrete-filled steel tubular structures. Liaoning, China; 2009 [in Chinese].
[21] EC4. Design of steel and concrete structures. Part 1-1: general rules and rules for building. EN 1994-1-1. Brussels, Belgium; 2004.
[22] Han LH. Flexural behaviour of concrete-filled steel tubes. Journal of Constructional Steel Research 2004;60(2):313–37.